Experimental investigations into capability of terahertz surface plasmons to bridge macroscopic air gaps

V. V. Gerasimov,[1,2,*] B. A. Knyazev,[1,2] A. K. Nikitin,[2,3] and G. N. Zhizhin[3]

[1]*Budker Institute of Nuclear Physics, Siberian Branch of Russian Academy of Sience, Novosibirsk, 630090, Russia*
[2]*Novosibirsk State University, Novosibirsk, 630090, Russia*
[3]*Scientific and Technological Center for Unique Instrumentatio, Russian Academy of Sience, 117342 Moscow, Russia*
[*]*einy@ngs.ru*

Abstract: Results of experimental and theoretical studies of the capability of terahertz surface plasmons (SPs) to cross macroscopic air gaps in a substrate (or between substrates) with admissible losses are presented. SPs were launched with quasi-cw free-electron laser radiation with 130 μm wavelength (λ). We managed to detect SPs passing across gaps as wide as 100 mm (or about $10^3 \cdot \lambda$), which is very promising for development of terahertz SP circuitry. The phenomenon was harnessed for splitting an SP beam into two new ones, guided by their own individual plane-surface substrates.

OCIS codes: (240.6680) Surface plasmons; (250.3140) Integrated optoelectronic circuits.

References and links

1. G. N. Zhizhin, M. A. Moskaleva, E. V. Shomina, and V. A. Yakovlev, "Surface electromagnetic wave propagation on metal surfaces," in *Surface Polaritons: Electromagnetic Waves at Surfaces and Interfaces*, V. M. Agranovich and D. L. Mills, ed. (North-Holland, 1982), Chap. 3.
2. S. A. Maier, *Plasmonics: Fundamentals and Applications* (Springer, 2007).
3. L. S. Mukina, M. M. Nazarov, and A. P. Shkurinov, "Propagation of THz plasmon pulse on corrugated and flat metal surface," Surf. Sci. **600**(20), 4771–4776 (2006).
4. V. V. Gerasimov, B. A. Knyazev, A. K. Nikitin, and G. N. Zhizhin, "A way to determine permittivity of real metal surfaces at terahertz frequencies," Appl. Phys. Lett. **98**(17), 171912 (2011).
5. G. N. Zhizhin, M. A. Moskalova, E. V. Shomina, and V. A. Yakovlev, "Edge effects due to propagation of surface IR electromagnetic waves along a metal surface," JETP Lett. **29**, 486 (1979).
6. S. P. Surov, Elements for middle IR SEW optics, Abstract of PhD thesis (Moscow, Prokhorov General Physics Institute, Russian Academy of Sciences, 1988), 20 p.
7. J. Seidel, F. I. Baida, L. Bischoff, B. Guizal, S. Grafstrom, D. V. Labeke, and L. M. Eng, "Coupling between surface plasmon modes on metal films," Phys. Rev. B **69**(12), 121405 (2004).
8. S. Sidorenko and O. J. F. Martin, "Resonant tunneling of surface plasmon-polaritons," Opt. Express **15**(10), 6380–6388 (2007).
9. R. A. Flynn, I. Vurgaftman, K. Bussmann, B. S. Simpkins, C. S. Kim, and J. P. Long, "Transmission efficiency of surface plasmon polaritons across gaps in gold waveguides," Appl. Phys. Lett. **96**(11), 111101 (2010).
10. M. I. Haftel, B. S. Dennis, V. Aksyuk, T. Su, and G. Blumberg, "Attenuation of surface plasmon intensity by transverse and longitudinal slits", ArXiv, http://girsh.rutgers.edu/Papers/Slit-strip_paper_7-18-12.pdf.
11. D. L. Begley, R. W. Alexander, C. A. Ward, R. Miller, and R. J. Bell, "Propagation distances of surface electromagnetic waves in the far infrared," Surf. Sci. **81**(1), 245–251 (1979).
12. E. S. Koteles and W. H. McNeill, "Far infrared surface plasmon propagation," Int. J. Infrared Millim. Waves **2**(2), 361–371 (1981).
13. J. Saxler, J. G. Rivas, C. Janke, H. P. M. Pellemans, P. H. Bolivar, and H. Kurz, "Time-domain measurements of surface plasmon polaritons in the terahertz frequency range," Phys. Rev. B **69**(15), 155427 (2004).
14. T.-I. Jeon and D. Grischkowsky, "THz Sommerfeld wave propagation on a single metal wire," Appl. Phys. Lett. **88**, 061113 (2006).
15. M. Nazarov, J.-L. Coutaz, A. Shkurinov, and F. Garet, "THz surface plasmon jump between two metal edges," Opt. Commun. **277**(1), 33–39 (2007).
16. M. Nazarov, F. Garet, D. Armand, A. Shkurinov, and J.-L. Coutaz, "Surface plasmon THz waves on gratings," C. R. Phys. **9**(2), 232–247 (2008).
17. V. B. Zon, "Reflection, refraction, and transformation into photons of surface plasmons on a metal wedge," J. Opt. Soc. Am. B **24**(8), 1960 (2007).

#251102 Received 29 Sep 2015; revised 17 Nov 2015; accepted 28 Nov 2015; published 17 Dec 2015

18. I. A. Kotelnikov, V. V. Gerasimov, and B. A. Knyazev, "Diffraction of surface wave on conducting rectangular wedge," Phys. Rev. A **87**(2), 023828 (2013).
19. V. V. Gerasimov, B. A. Knyazev, I. A. Kotelnikov, A. K. Nikitin, V. S. Cherkassky, G. N. Kulipanov, and G. N. Zhizhin, "Surface plasmon polaritons launched using a terahertz free electron laser: propagating along a gold-ZnS-air interface and decoupling to free waves at the surface tail end," J. Opt. Soc. Am. B **30**(8), 2182 (2013).
20. R. G. Hunsperger, *Integrated Optics: Theory and Technology*. 5th ed. (Springer-Verlag, 2002), Chap. 7–8.
21. B. A. Knyazev and A. V. Kuzmin, "Surface electromagnetic waves: from visible range to microwaves," Vestn. Novosib. State Univ. Phys. **2**, 108–122 (2007).
22. B. A. Knyazev, G. N. Kulipanov, and N. A. Vinokurov, "Novosibirsk terahertz free electron laser: instrumentation development and experimental achievements," Meas. Sci. Technol. **21**(5), 054017 (2010).
23. G. I. Stegeman, R. F. Wallis, and A. A. Maradudin, "Excitation of surface polaritons by end-fire coupling," Opt. Lett. **8**(7), 386–388 (1983).
24. K. Hasegawa, J. U. Nöckel, and M. Deutsch, "Curvature-induced radiation of surface plasmon polaritons propagating around bends," Phys. Rev. A **75**(6), 063816 (2007).
25. M. A. Dem'yanenko, D. G. Esaev, B. A. Knyazev, G. N. Kulipanov, and N. A. Vinokurov, "Imaging with a 90 frames/s microbolometer focal plane array and high-power terahertz free electron laser," Appl. Phys. Lett. **92**(13), 131116 (2008).
26. M. A. Dem'yanenko, D. G. Esaev, I. V. Marchishin, V. N. Ovsyuk, B. I. Fomin, B. A. Knyazev, and V. V. Gerasimov, "Application of uncooled microbolometer detector arrays for recording radiation of the terahertz spectral range," Optoelectron. Instrum. Data Process. **47**(5), 508–512 (2011).
27. V. V. Gerasimov, B. A. Knyazev, A. K. Nikitin, and V. V. Nikitin, "Method for identifying diffraction satellites of surface plasmons in terahertz frequency range," Tech. Phys. Lett. **36**(11), 1016–1019 (2010).
28. M. A. Ordal, L. L. Long, R. J. Bell, S. E. Bell, R. R. Bell, R. W. Alexander, Jr., and C. A. Ward, "Optical properties of the metals Al, Co, Cu, Au, Fe, Pb, Ni, Pd, Pt, Ag, Ti, and W in the infrared and far infrared," Appl. Opt. **22**(7), 1099–2220 (1983).
29. B. A. Knyazev, A. K. Nikitin, G. N. Zhizhin. Method for conjugating a set of secondary plasmon-polaritions communication channels of the terahertz spectral range with the basic one, Patent of Russia No. 2526888, 27.08.2014.
30. "THz Beam Splitters", THz Beam Splitters Datasheet, *http://www.tydexoptics.com/en/products/thz_optics/thz_beam_splitter/*

1. Introduction

Adherence to Surface plasmons (SPs) play an important role in photonic devices in the visible and near-infrared (IR) spectral regions [1,2]. In the mid-IR and terahertz (THz) ranges, SPs have a great potential of applications in surface spectroscopy and optical communication, because their propagation length, in contrast to short-wavelength SPs, is macroscopic and equals to centimeters and, under proper conditions, even to tens of centimeters [3,4]. To employ SPs in communication and information processing devices, one has to solve the problem of signal transmission from one module to another. The simplest way of building interfaces of SP communication channels may be transmission of SP beams across air gaps with reasonable loss. This is one of the motives for studying the phenomenon of the "jumping" performed by SPs. Such study is also valuable for a number of other applications: (1) IR and THz SP spectrometers, where plug-in samples are placed between stationary plane-surface SP waveguides; (2) splitting, deflection, and focusing of SP beams; (3) SP sensing etc.

The phenomenon of SP "jumping" across air gaps was discovered by one of the authors in 1979 for SPs generated by a CO_2 laser (λ = 10.6 μm) on thick aluminum films evaporated onto plane glass substrates [5]. In those experiments, the SPs crossed *mm*-wide through scratches in the film, the intensity damping approximately linearly proportional to the scratch width. For example, the SPs bridged the largest scratch (6 mm wide), their intensity decreasing 6 times only. Later on, a closer look at the science behind the phenomenon was taken in the PhD thesis by S.P. Surov [6]. He stated that the maximum transmission efficiency could be attained when the guiding surface of the receiving sample was slightly shifted up horizontally relative to the guiding surface of the transmitting sample.

The jumping of visible and near-IR plasmons was studied in many recent papers devoted to nanoplasmonic circuitry. As examples we can mention papers [7–10], in which jumps of SPs were studied theoretically and/or experimentally using different techniques, including the far-field and near-field microscopy. The characteristic gap widths were within 10 μm. For instance, R.A. Flynn et al. [9] found that at λ = 860 nm the intensity of SPs passing across gaps in a gold film was close to 100% of its initial value for a 30-nm air gap and remained as

#251102 Received 29 Sep 2015; revised 17 Nov 2015; accepted 28 Nov 2015; published 17 Dec 2015

high as 50% for a 1-μm gap. The rest of the power radiated into the substrate and air above the film, only a few percent reflected into the SP mode propagating backwards.

The study of SP transmission across gaps in the terahertz spectral range was started rather recently. Though pioneer experimental studies on excitation of THz SPs at metal-dielectric interfaces were performed using radiation of gas lasers in the late 1970s [11,12], after the development of the time-domain spectroscopy (TDS) technique, practically all recent experiments with THz SPs were performed using wideband radiation sources (see, for example [13–16],). Using the TDS technique is beneficial in many respects, but this method has obvious pitfalls of dispersion origin when SPs are under study. Using monochromatic radiation, one can avoid problems with dispersion of broadband THz SPs, uncertainty in phase shifts at coupling and decoupling elements, as well as the necessity of the inverse Fourier transform in data processing.

In this paper we describe experiments on the transmission of "monochromatic" THz plasmons across air gaps between mating arched rectangular ends of two plane metal-dielectric samples, used for coupling incident radiation with SPs on the transmitting sample and for converting SPs into bulk radiation on the target sample. The arched ends shielded the detector from stray emission.

2. Brief theory and computational modeling

To develop an analytical model of SP transmission across an air gap between plane guiding structures one has to consider two stages of the process: 1) diffraction of SPs on the edge of the transmitting structure (sample), which results in production of a bulk wave (BW) with its radiation pattern dependent on the distance from the edge; 2) excitation of SPs on the edge of the receiving (target) sample by the BW emitted by the SPs on the first sample.

To simplify the problem, let us suppose that the mating edges of both samples have a rectangular form, and their SP-guiding surfaces are oriented in the horizontal plane and not limited in the direction normal to the plane containing the SP track (Fig. 1).

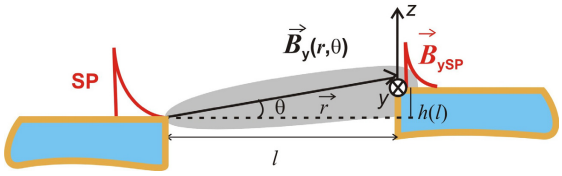

Fig. 1. Diagram of SP bridging over air gap between two samples with rectangular edges.

The problem of SP diffraction on a rectangular edge of a metal sample was thoroughly considered in a number of papers [17,18]. It was stated that practically all the SP energy incident on the edge is converted into the energy of the diffracted BW.

At small distances r from the edge (near-field wave zone), the BW field is still strongly influenced by the fields of free charges oscillating on the surface of the transmitting sample. At distances $r > k_o^{-1} \cdot \left|\mathrm{Im}\left[\arcsin(\xi)\right]\right|^{-2}$, where $k_o = 2\pi/\lambda$ and ξ is the surface impedance of the SP-guiding structure, the BW becomes self-sustained and acquires all features inherent to a free wave propagating in a surrounding medium (far-field wave zone) [18]. Note that for a metal surface covered with a dielectric layer of thickness d the value of ξ can be estimated by approximate formula (11) in [18],

$$\xi \cong \frac{1}{\sqrt{\varepsilon_m}} - i \cdot \frac{\varepsilon_d - 1}{\varepsilon_d} \cdot k_o \cdot d, \qquad (1)$$

#251102 Received 29 Sep 2015; revised 17 Nov 2015; accepted 28 Nov 2015; published 17 Dec 2015

where ε_m and ε_d are the dielectric permittivity of the metal and the dielectric, respectively; i is the imaginary unit. Equation (1) is valid under the conditions $|\varepsilon_m| >> 1$ and $\left(k_o \cdot \sqrt{|\varepsilon_m|}\right)^{-1} << d << \lambda$, which are well met for most metals in the THz range.

Kotelnikov I.A. and coauthors [18] obtained an analytical expression for the diffracted BW field in terms of its transverse magnetic component,

$$B_y(r,\theta) = -exp\left(-s^2\right) \cdot \left[-1 + i \cdot erfi(s)\right] \cdot exp\left(ik_o r\right)/2, \quad (2)$$

where $erfi(s) = \left(2/\sqrt{\pi}\right) \cdot \int_0^s exp\left(t^2\right) dt$ is the imaginary error function; $s = (1+i) \cdot \left[\theta + arc\sin(\xi)\right] \cdot \sqrt{k_o \cdot r}/2$; θ is the angle of inclination of the BW radiation pattern maximum to the plane of the transmitting sample (see Fig. 1).

Formula (2) is valid for any distance r, i.e. both for the near- and far-field wave zones. Its validity was tested in the THz range with monochromatic SPs excited by free-electron laser (FTL) radiation with λ = 130 μm on gold-evaporated optically-polished plane glass samples with a rectangular edge [19]. The correlation between the measured distributions of the BW intensity at various distances r and those calculated employing formula (2) was quite satisfactory.

Since practically all the SP energy is converted into the energy of the diffracted BW, the SP transmission efficiency between two conducting surfaces is almost totally defined by the efficiency η *of* coupling of a bulk diffracted wave to a surface plasmon on a receiving sample edge (hereinafter η is the transmission efficiency). To estimate the value of η it is sufficient to find the overlapping [20] of the tangential components of the magnetic fields of the waves [21],

$$\eta = \frac{\left| \int_0^\infty \int_{-\infty}^\infty B_y(y,z) \cdot B_{ySP}^*(y,z)\, dydz \right|^2}{\int_0^\infty \int_{-\infty}^\infty \left|B_y(y,z)\right|^2 dydz \cdot \int_0^\infty \int_{-\infty}^\infty \left|B_{ySP}^*(y,z)\right|^2 dydz}, \quad (3)$$

here $B_y(y,z)$ is the magnetic field of the diffracting SP wave on the transmitting sample; $B_{ySP}^*(y,z)$ is the complex conjugate magnetic field of the SP wave on the receiving sample. Note that the integration is carried out in the upper (y, z) half-plane (see Fig. 1), and the overlap integral is normalized to the intensities of the corresponding magnetic fields (denominator of Eq. (3)).

In our case, the dependencies of $B_y(y,z)$ and $B_{ySP}^*(y,z)$ on the coordinate y are defined by the Gaussian profile of the FEL beam intensity, which is proportional to $exp\left(-2y^2/w_b^2\right)$, where w_b is the waist of the beam. Under this condition, the two-dimensional integrals in Eq. (3) can be split into one-dimensional integrals, and Eq. (3) acquires the following simplified form:

$$\eta = \frac{\left| \int_0^\infty B_y(z) \cdot B_{ySP}^*(z)\, dz \right|^2}{\int_0^\infty \left|B_y(z)\right|^2 dz \cdot \int_0^\infty \left|B_{ySP}^*(z)\right|^2 dz}, \quad (4)$$

#251102 Received 29 Sep 2015; revised 17 Nov 2015; accepted 28 Nov 2015; published 17 Dec 2015

where the quantity $B_y(z)$ should be estimated by formula (2) with $r=\sqrt{l^2+(h+z)^2}$ and $\theta = a\tan\left[(h+z)/l\right]$; l is the width of the gap between the transmitting and receiving samples; $h = l{\cdot}tan(\theta_{max})$ is the shift of the receiving sample upwards along the axis z to the coordinate where the transmitting sample radiation pattern attains a maximum; $B^*_{ySP}(z) = B_{0y}\cdot\exp(-z/\delta)$ is the SP field at edge of the receiving sample; δ is the depth of SP field penetration into the surrounding medium, e.g. air.

Figure 2(a) presents the results of a computational modeling of the radiation patterns, calculated by Eq. (4) using MathCAD software for SPs with λ = 130 μm on gold (*Au*) samples covered with a zinc sulfide (*ZnS*) layer 1.5 μm thick and for various distances l from the radiating sample edge. One can see that at any l the pattern achieves a maximum intensity at an appropriate angle θ_{max}, and the larger is l, the smaller is θ_{max}. Analyzing the patterns for l varying from 1 to 70 mm, we found the dependency $\theta_{max}(l)$ (see Fig. 2(b)), which was approximated by power functions in the near-field zone (l≈1-15 мм) and the far-field zone (l≈15-70 мм). Afterwards these approximation functions were used for determination of the $h(l)$ dependency.

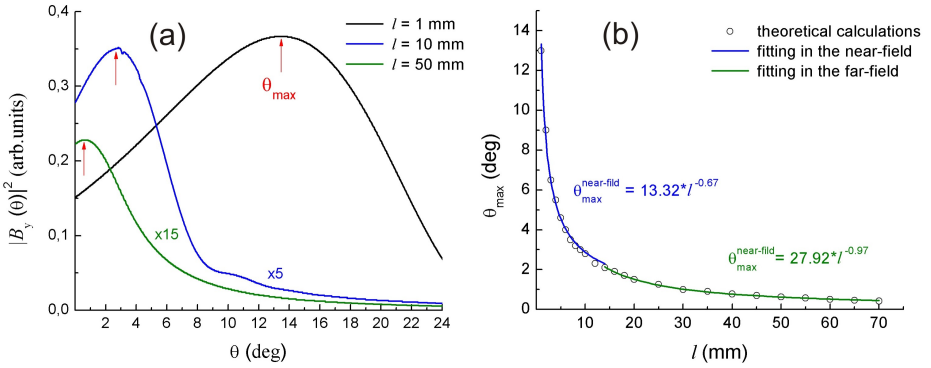

Fig. 2. Calculation of radiation patterns of bulk wave produced by SPs diffracting on rectangular edge of *Au* sample covered with *ZnS* layer 1.5 μm thick: (a) field intensity $|B_y|^2$ dependencies on angle θ measured from the sample plane at various distances l from the edge; (b) dependency of angle θ_{max} (pattern maximum intensity) on distance l (circles: calculated θ_{max} values; solid lines: results of computational fitting).

Dependencies of the transmission efficiency coefficient η on the air gap size l (in the range of 2 to 70 mm) calculated for an *Au* transmitting sample covered with a *ZnS* layer of thickness d_1 = 1.5 μm and for an *Au* receiving sample covered with a *ZnS* layer of another thickness d_2 for λ = 130 μm are plotted in Fig. 3. In the near-field zone (l<15 mm) η decreases with l monotonously, and the slopes of all the curves are approximately the same. In the far-field zone (l>15 mm) the slopes become different: the larger is d_2 the greater slopes are. Such behavior of $\eta(l)$ dependencies can be understood if one takes into consideration that SP decay length at the receiving sample decreases with growth of the dielectric layer thickness (δ~1/d_2), reducing the overlap integral in Eq. (4).

#251102 Received 29 Sep 2015; revised 17 Nov 2015; accepted 28 Nov 2015; published 17 Dec 2015

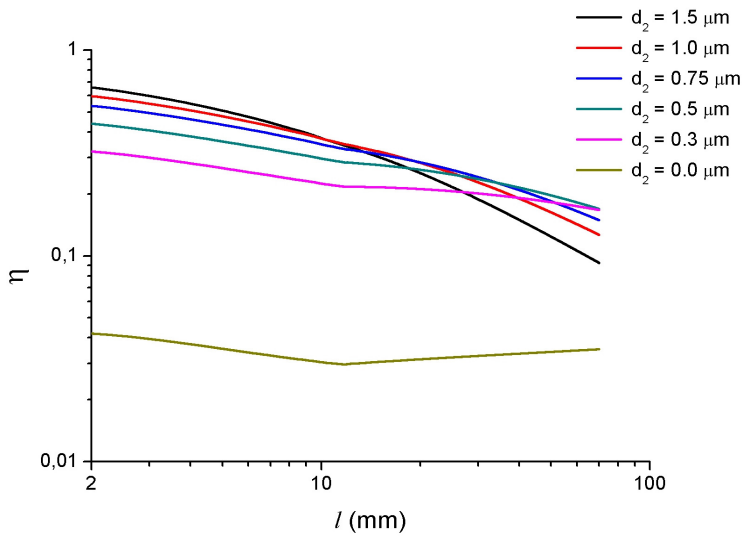

Fig. 3. Theoretical calculation of dependency of SP transmission efficiency η on air gap length l between transmitting sample with *ZnS* layer 1.5 μm thick on its surface and receiving sample with *ZnS* layer of another thickness d_2 = 0.0, 0.3, 0.5, 0.75, 1.0 and 1.5 μm.

Plots in Fig. 4 demonstrate that for each distance l spacing the samples there is an optimal thickness d_2^* of the dielectric coverage with which the SP transmission efficiency η attains a maximum; besides, the larger is l, the more pronounced is this effect and the smaller is d_2^*.

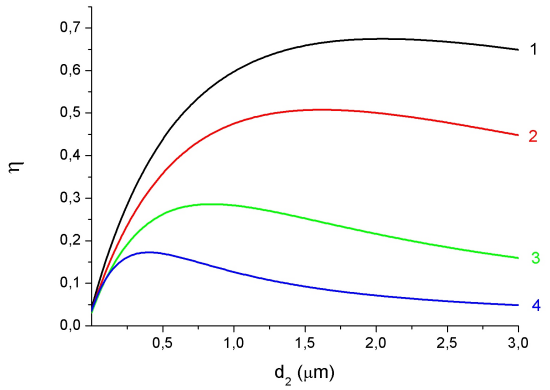

Fig. 4. SP transmission efficiency η between two *Au* samples vs. receiving sample *ZnS* coverage thickness d_2, calculated for various air gap sizes l (the thickness of the *ZnS* layer on the transmitting sample is constant and equals 1.5 μm). 1: l = 2; 2: l = 5; 3: l = 20; 4: l = 70 mm.

3. Experimental setup and samples

The experiments were carried out at the SPIN user station of the Novosibirsk free electron laser (NovoFEL) facility [22] at a fixed wavelength λ = 130 μm (f = 2.3 THz) with the spectral line width less than 1%. There is practically no radiation absorption in air with this wavelength. The laser generated a continuous stream of 100-*ps* pulses ($c\cdot\tau\approx$30 mm) with a repetition rate of 5.6 MHz. The characteristic beam average power in the experiments was about 10 W.

The experimental diagram is shown in Fig. 5. We favored the end-fire coupling technique [23] for transforming the FEL radiation into SPs as a simpler, more effective (up to 90%

#251102 Received 29 Sep 2015; revised 17 Nov 2015; accepted 28 Nov 2015; published 17 Dec 2015

efficiency) and reliable one. In contrast to the classical implementation of the method, involving SP excitation by bulk waves diffracting on a rectangular edge of a plane-surface substrate, we used for this purpose the edge of the curved surface of a quarter of a glass cylinder used as a transmitting sample. A cylindrical mirror with a focal distance of 12.5 cm condensed an FEL beam of about 10 mm in diameter in a line. The focused radiation fell onto the edge of the quarter-cylinder and due to diffraction excited SPs on its gold-metalized curved surface. The radius of the surface (60 mm) exceeded λ many folds, which reduced the curvature contribution to SP radiative losses [24]. For the sake of higher coupling efficiency, the cylinder surface was covered with a 1.5 μm thick *ZnS* layer. What is more important, the cylindrical form of the coupling element made it an effective screen, shielding the photo detector from diffracted parasitic bulk waves.

As for the target (receiving) sample, it was a bar with its output end 4 cm long cut at an angle of 13 degrees; both the SP guiding surfaces of the target sample 10 cm long were connected by a conjugation edge with a radius of 10 mm (this method of detector screening in THz SP science was first suggested in [12]). The SP guiding surfaces of the sample were covered with a ZnS layer of thickness d, varying from sample to sample in the range of 0 to 1.5 μm.

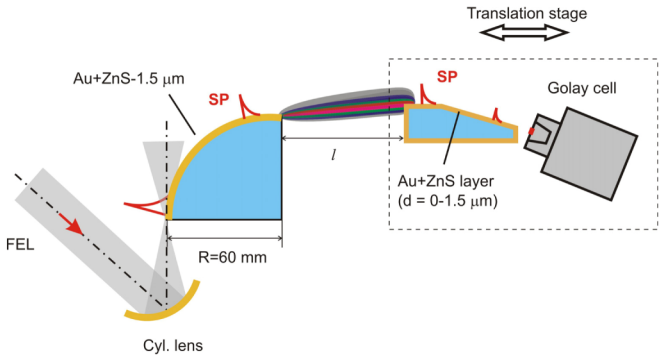

Fig. 5. Schema of the experimental setup.

We recorded the SP intensity with two THz radiation sensors at the output end of the target sample: an imaging system consisting of a microbolometer focal plane array [25,26] (MBFPA) equipped with a TPX lens and an optoacoustic detector (GC-1T Golay cell, TYDEX, J. S. Co). The Golay cell (NEP = 1.4×10^{-10} W/Hz$^{1/2}$) with an entrance slit 0.2 mm wide parallel to the guiding surface was connected to a Stanford Research SR-830 lock-in amplifier. In the latter case, the input radiation was chopped at an optimal frequency of 15 Hz.

4. Results and discussions

First we registered (with both the photo detectors placed at a distance l = 50 mm) the intensity distribution of the bulk radiation produced by SPs diffracting at the output edge of the transmitting sample (Fig. 6). In good correlation with the theory [18], the radiation diagram had a pronounced narrow main peak with an angular width of about 5° at half the maximum intensity; the peak was slightly inclined ($\theta \approx 1.0°$) upwards relative to the tangent line drawn to the output edge of the sample. The satellite peaks observed on the diagram are typical to the near wave zone, stretching up to tens of millimeters depending on the *ZnS* layer thickness. Note that according to [18], the thicker is the *ZnS* layer, the broader is the radiation diagram and the smaller is its slope angle θ. In all the subsequent measurements (at any distance l spacing the samples), the entrance slit of the Golay cell was centered at the maximum of the transmitting sample radiation diagram.

On the second stage of the study we jointed the ends of the samples, making l = 0, and investigated the SP capability to overcome an impedance step at the junction between samples with *ZnS* coverage of different thickness *d*. The detectors were placed (or were scanning in

#251102 Received 29 Sep 2015; revised 17 Nov 2015; accepted 28 Nov 2015; published 17 Dec 2015

case of the Golay cell) in the immediate vicinity of the output end of the target sample. To make sure that the photocurrent was produced by the SPs, not by parasitic beams, we practiced a very simple and reliable method suggested in [27]. A paper strip was placed on the sample surface across the SP track. If the current is produced by the SPs, the strip at any part of the track must change the photocurrent I measured at any particular point of the track (e.g. at the end of the sample) by the same amount. In case the current is produced by bulk waves reflected from the sample surface, its force depends on the strip location. In the experiments we put a paper strip 20 mm wide on various parts of the receiving sample surface, including its slope, and found out that with any position of the strip the value of I dropped about tenfold. A supplementary test assumed a change in the radiation polarization: when a p polarization was switched to an s one, the signal vanished to the noise level. So there was no doubt that we dealt with SPs, not with anything else.

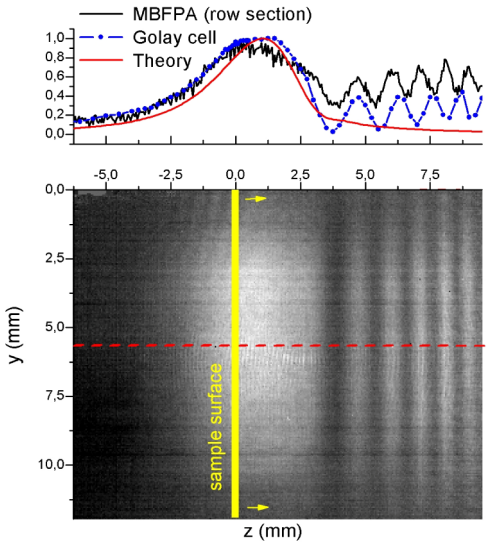

Fig. 6. Distribution of intensity of bulk radiation produced by SPs at edge of transmitting cylindrical sample and recorded with 1) Golay cell (top), solid red line: computational modeling; 2) microbolometer MBFPA (bottom), dashed red line: plane of cell scanning.

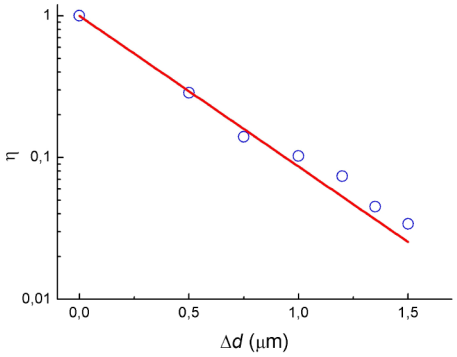

Fig. 7. SP transmittance η through joint between transmitting and receiving samples vs. difference Δd in thicknesses of ZnS coverage layers. Circles: experiment; solid red line: exponential approximation.

Figure 7 presents the experimental dependency of the SP transmission η, obtained for the samples brought into immediate contact ($l = 0$) on the difference Δd in the thicknesses of the ZnS layers of the transmitting and receiving samples. One can see that the smaller is the

#251102 Received 29 Sep 2015; revised 17 Nov 2015; accepted 28 Nov 2015; published 17 Dec 2015

difference in the samples coverage thickness, the greater is the percentage of the SP field energy passed through the barrier, reaching 100% transmittance when the *ZnS* layers on both samples had the same thickness d = 1.5 μm. The recorded dependency $I(d)$ has almost an exponential character. Note that in the experiments we ignored the dependence of the SP extinction on the *ZnS* layer thickness d on the receiving samples, as their dimensions were much smaller in comparison with the SP propagation length.

After that we recorded the SPs intensity I at the end of the target sample, increasing the gap between the samples and adjusting the target sample to a maximum signal by moving it along the z-axis at each distance l. As the coupling conditions and the transmitting sample itself remained stable and permanent in the experiments, the diffracted bulk wave produced by the SPs at the source sample end was the same for all target samples with different *ZnS* coverages. So, one can conclude that the capability of SPs to cross an air gap of a particular size was mainly defined by the efficiency of the bulk wave to couple with SPs on a target (receiving) sample. The obtained dependencies $\eta = I(l)/I_0$ for receiving samples with various *ZnS* layers are presented in Fig. 8, here I_0 is the signal detected at the end of the target sample with 1.5 μm thick *ZnS* layer in case of zero gap (l = 0), that insures 100% of the SP transmission efficiency (see Fig. 7). In the near-field zone (l<15 mm) the SP bridging efficiency η drops at approximately the same rate for all receiving samples, which correlates with calculations made for the near-field zone (see Fig. 3). For gaps with l>15 mm the efficiency η decays for smaller d_2 less rapidly. Again, this fact could be interpreted in terms of the fields overlap integral: for smaller values of d_2 the SP field penetration depth δ into air is greater, that makes η less sensitive to the gap size l variations. This tendency of $\eta(l)$ dependencies in the far-field wave zone is more pronounced on the calculated plots depicted in Fig. 3.

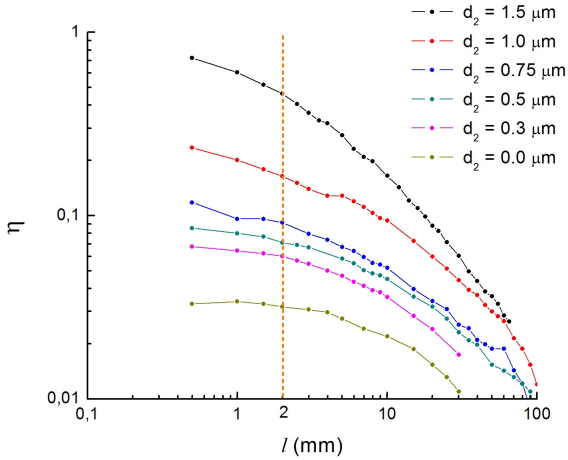

Fig. 8. SP transmission efficiency η between transmitting *Au* sample with *ZnS* coverage d_1 = 1.5 μm thick and receiving *Au* samples with *ZnS* coverage of various thicknesses d_2 vs. the gap size l. The dash line at l = 2 mm depictes the left border of calculated dependencies $\eta(l)$ shown in Fig. 3.

Finally we performed experiments on the SP capability to "jump" between *Au* samples with an identical *ZnS* coverage thickness of 1.5 μm on both the transmitting sample and the receiving one. Results of the measurements are presented in Fig. 9. Here the experimental values of the transmission efficiency η are depicted with circles, and the fitting and dependencies $\eta(l)$ calculated with Eq. (4) are shown with the blue and red lines, respectively. In the far-field wave zones, the experimental points were approximated by a power function, like $a \cdot l^{-b}$, where index b was equal to 0.94 ± 0.06. As the b values are rather close to unity, one can say that in the far-field wave zone the efficiency η of SP transmission between two

#251102 Received 29 Sep 2015; revised 17 Nov 2015; accepted 28 Nov 2015; published 17 Dec 2015

identical conducting surfaces is inversely proportional to *l*. This fact can be accounted for by the quasi cylindrical form of the bulk wave produced by the SPs when diffracting on the transmitting sample edge.

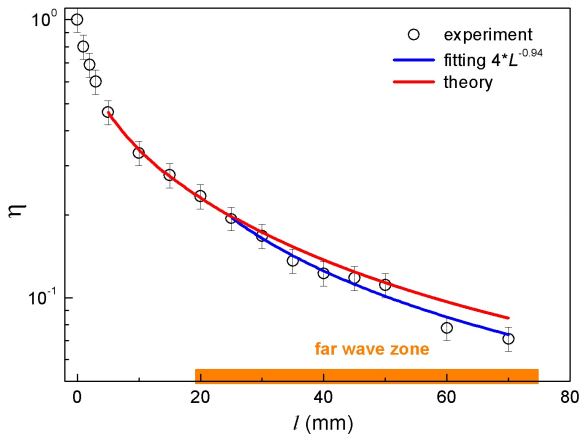

Fig. 9. Experimental and theoretical SP transmission efficiency η dependencies on air gap size l for two *Au* samples with identical *ZnS* coverage layer thickness d = 1.5 μm.

To conclude, we compare in Table 1 the length of the plasmon jumping in different spectral ranges, in absolute values and those normalized to the wavelength (λ). Whereas shortwave plasmons can bridge only small gaps, SPs in the wavelength range of 5 –150 μm show a capability to bridge gaps as large as 100 mm, which exceeds λ by three orders of magnitude. Taken together with the rather large propagation lengths (centimeters and tens of centimeters), though they are nearly two orders of magnitude less than those calculated with the Drude model [28], and the SP capability to follow curved surfaces, this is very beneficial for development of SP bio-chips, integrated circuits and surface examination. It is clearly seen from Table 1 that there is a "blank spot" in the investigations into SPs, namely the spectral range between 10 and 130 μm. Study of plasmon characteristics within the region λ = 30-80 μm, which is now available at the NovoFEL facility, might be helpful in explaining the discrepancy with the Drude theory and understanding the feasibility of using this region in plasmonics.

Table 1. SP transmission through air gaps in spectral range from near-IR to sub-mm

Surface	λ, μm	$L_{1/e}$, μm	$l_{1/e}/\lambda^a$	Ref.
Au	0.73	0.9	1.2	10
Au	0.86	2	2.4	9
Al	10	2000	200	5
Au + 0.5 μm ZnS	130	86000	660	This paper
Au + 1.5 μm ZnS	130	43000	330	This paper
DurAl	630	20000	32	16

[a]Here $l_{1/e}$ is the gap width corresponding to the damping of the SP intensity by the factor *e*.

5. Use of SP "jumping" capability for splitting of SP beam

One of the obvious applications of the SP capability to bridge macroscopic air gaps is the splitting of SP communication channels [29]. The idea is illustrated by the sketch in Fig. 10. SPs of the basic channel diffract on its substrate edge and turn into a set of bulk waves (BWs) with a rather narrow radiation pattern. These BWs fall onto a beam-splitting plate placed normally to the plane of the basic channel SP-guiding facet and at some angle β to the SP track. The plate divides the BWs into two parts (transmitted and reflected, BW-1 and BW-2), the intensity proportion depending on β, the refractive index and the thickness of the plate. Both secondary waves preserve the identity of the initial BWs and are capable to effectively

#251102 Received 29 Sep 2015; revised 17 Nov 2015; accepted 28 Nov 2015; published 17 Dec 2015

excite SPs on rectangular edges of other metal (metalized) substrates. Appropriate substrates are disposed in a plane parallel to the SP-guiding facet of the basic channel, a bit above it, for fitting the maximum of the radiation pattern. Besides, one of the substrates is oriented along the SP track, while the other can be directed at any angle to the track (e.g. at the right one). On reaching the front edges of the substrates, BW-1 and BW-2 excite SP-1 and SP-2, accordingly, on them. This is an obvious way for multiplexing of THz SP channels.

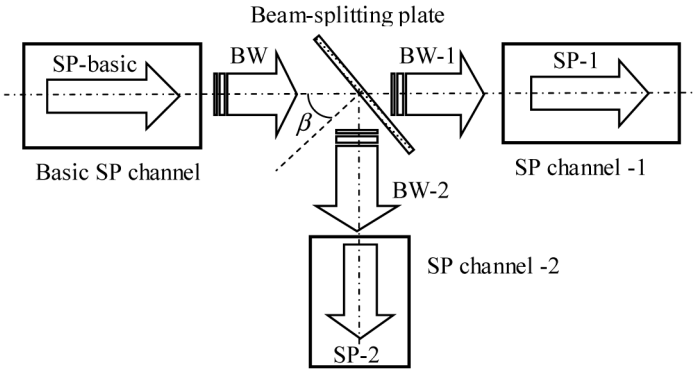

Fig. 10. Design of setup for multiplexing of THz SP communication channels.

We performed measurements illustrating the possibility of multiplexing of THz SPs employing their capability to bridge macroscopic air gaps. A scheme of the experimental setup used for the measurements is represented in Fig. 11. The SPs were launched on a plane sample 150 mm long (containing a nontransparent gold film covered with a *ZnS* layer 0.57 μm thick) in the same way as in section 3. The only exception was that an eighth part of the glass cylinder instead of a quarter-cylinder was used for coupling of the FEL radiation and the SPs, as a 45° segment was quite sufficient for shielding the photodetector from parasitic bulk waves. A subsidiary metal screen was placed at a distance of 15 mm from the junction between the coupling element and the sample, its edge spaced by 5 mm from the sample surface to absorb bulk waves produced by the SPs due to their diffraction at the junction. The receiving sample was identical to the coupling element, but its golden cylindrical surface had a *ZnS* coverage 0.5 μm thick. A Golay cell combined with a 15 Hz chopper and a lock-in amplifier was used for radiation sensing, while a high-resistivity silicon plate 1 mm thick served as a beam splitter [30].

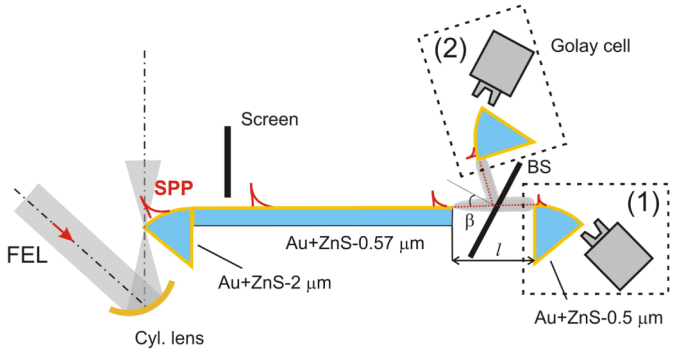

Fig. 11. Scheme of the setup used for multiplexing of THz SPs: (1) transmission channel; (2) reflectance channel.

First we detected signal right at the sample plate end opposite to its counterpart adjoining the coupling element. Having run 150 mm along the plane and some distance along the receiving cylindrical surface, the SPs diffracted on the end's edge and entered the input

#251102 Received 29 Sep 2015; revised 17 Nov 2015; accepted 28 Nov 2015; published 17 Dec 2015

window of the Golay cell. When the detector was removed from the sample end to a distance l = 50 mm and placed in a position corresponding to the maximum of the radiation pattern, the output signal dropped to 32% from its value at l = 0.

Then the silicon plate beam splitter was placed into the spacing between the transmitting and receiving samples and positioned with an incidence angle $\beta = 30°$, which provided approximately equal reflectance and transmission coefficients of the plate . The signals detected for positions (1) and (2) of the unit "Receiving sample - Golay cell" (see Fig. 11) at the same distance l = 50 mm run by the radiation in air turned out to be equal as well. Thus, we realized duplication of SP communication channel employing the SP capability to cross macroscopic air gaps.

6. Conclusion

We have demonstrated that monochromatic terahertz (THz) surface plasmons (SPs) guided by golden plane substrates covered with sub-micron-thick zinc sulfide layers can cross macroscopic air gaps 100 mm wide. A new coupling element with a cylindrical SP guiding surface was tested for implementing the end-fire coupling technique; the element enables thorough interception of diffracted bulk waves, which safely shields the photodetector from parasitic exposures. The theoretical calculations of the SP transmission efficiency were in good qualitative correlation with the experiments. A THz SP beam splitter based on the "jumping" capability of SPs was designed and tested using free-electron laser radiation with a 130 μm wavelength. The phenomenon of "jumping" of SPs is rather promising for terahertz SP circuitry development.

Acknowledgments

The experiments performed at the Novosibirsk free electron laser facility were supported by the Russian Science Foundation (N 14-50-00080). The experiments were carried out with equipment belonging to the Siberian Centre of Synchrotron and Terahertz Radiation. The authors are indebted to G. N. Kulipanov and N. A. Vinokurov for their support in this work, and to the Novosibirsk free electron laser facility operation team.

#251102 Received 29 Sep 2015; revised 17 Nov 2015; accepted 28 Nov 2015; published 17 Dec 2015